Combining Multicomponent Seismic Attributes, New Rock Physics Models, and In Situ Data to Estimate Gas-Hydrate Concentrations in Deep-Water, Near-Seafloor Strata of the Gulf of Mexico

Semi-Annual Report
Due Date: 30 September 2007

Reporting Period Start Date: 1 March 2006

Reporting Period End Date: 30 September 2007

Principal Investigators: Bob A. Hardage
Paul E. Murray
Diana C. Sava

Report Date: 24 October 2007

DOE Award DE-FC26-05NT42667

Submitting Organization: Bureau of Economic Geology
The University of Texas at Austin
University Station, Box X
Austin, TX 78713-8924

Disclaimer

This report was prepared as an account of work sponsored by an agency of the United States Government. Neither the United States Government nor any agency thereof, nor any of their employees, makes any warranty, express or implied, or assumes any legal liability or responsibility for the accuracy, completeness, or usefulness of any information, apparatus, product, or process disclosed, or represents that its use would not infringe privately owned rights. Reference herein to any specific commercial product, process, or service by trade name, trademark, manufacturer, or otherwise does not necessarily constitute or imply its endorsement, recommendation, or favoring by the United States Government or any agency thereof. The views and opinions of authors expressed herein do not necessarily state or reflect those of the United States Government or any agency thereof.

Abstract

Gas hydrate research being done at the Bureau of Economic Geology through DOE Award DE-FC26-05NT42667 has completed Task 1 through Task 8 and is on schedule. This semi-annual report describes the team's latest work on Task 8 in which we developed a rock physics theory for deep-water, near-seafloor sediment that relates interval values of seismic-derived P-wave and S-wave velocities to hydrate concentration within these sediments. This report describes our theory and shows that our theoretical predictions match laboratory measurements of P and S velocities performed on man-made mixtures of hydrate and sediment that approximate physical conditions (porosity, effective pressure, and temperature) found in deep-water, near-seafloor environments.

Table of Contents

List of Figures

Introduction

Rock physics models are presented describing hydrate systems associated with deep-water unconsolidated marine sediments. Our goals are to predict hydrate concentration from seismic P- and S-wave velocities, and to analyze P-P and P-SV reflectivity at the base of hydrate stability zones. Elastic moduli of hydrate systems depend on: (1) elastic moduli of the sediments that host the hydrates, (2) elastic moduli of the hydrates that are mixed with the sediments, (3) concentration of hydrates in the sediments, and (4) the geometrical details of the distribution of hydrates within their host sediments. We consider the following four scenarios for hydrate occurrence: load-bearing hydrate, pore-filling hydrate, and two different models of thin hydrate layers intercalated with thin layers of hydrate-free sediments. A key finding of our theory is that the geometrical details of how hydrates are distributed within deep-water sediments control the relationships between hydrate concentration and seismic velocities. We conclude that to produce accurate estimates of deep-water hydrate concentrations from seismic data, we need to know how to describe the geometrical patterns in which hydrate occurs at study sites. Our modeling results for thin-layered hydrate morphologies show significant S-wave anisotropy. This finding encourages us that by using multicomponent seismic data we may be able to infer when hydrate is distributed as alternating thin layers of hydrate-bearing sediments and hydrate-free layers. In addition, if the thin layers are aligned and vertical, approximating fractures and veins filled with pure hydrate, the seismic response is azimuthally dependent, which enables us to identify this type of distribution and to quantify the hydrate concentration.

We compare our theoretical P-wave and S-wave velocity predictions with published laboratory measurements of V_P and V_S made on load-bearing synthetic hydrate formed in unconsolidated sand and clay. We find good agreement between our predicted velocity values for disseminated, load-bearing hydrate and these laboratory measurements. We consider this agreement to be a confirmation that our theory is valid.

Executive Summary

Our goal of rock physics modeling of marine-hydrate systems is to infer hydrate concentration in seafloor sediment from seismic measurements. Many published relations between hydrate concentration and seismic attributes are empirical (Pearson et al., 1983; Miller et al., 1991; Wood et al., 1994; Holbrook et al., 1996; Lee et al., 1996; Yuan et al., 1996; Collett, 1998; Lu and McMechan, 2002, 2004). Empirical approaches are easy to implement, but they do not have predictive power and should be used only at the specific site where the relationships are derived. More important, empirical relations do not provide insights into the morphological character of how gas hydrates are distributed within sediments.

There are studies that use physics-based effective-medium models of hydrate systems to relate hydrate concentration to seismic properties (Helgerud et al., 1999; Ecker et al., 2000; Carcione and Tinivella, 2000; Chand et al., 2004; Winters et al.,

2004; Waite, et al., 2004; Kleinberg and Dai, 2005; Murray et al., 2006). Some of these effective-medium models are based on Dvorkin and Nur's (1996) model of unconsolidated sediments, which uses Hertz-Mindlin's theory (Mindlin, 1949; Mavko et al., 1998). These models are appropriate for relatively deep marine sediments (>300 mbsf), but they do not explain lab observations or in-situ observations made within the first 200 meters below the seafloor where sediments have low shear strengths, large V_P/V_S ratio, and almost zero effective pressure.

There is a need for improved rock physics models that can characterize seismic velocity behavior in unconsolidated sediments within deep-water, near-seafloor strata where hydrates may be present. Rock physics models are also needed to help understand how hydrates are distributed relative to their host sediments. Are the hydrates disseminated as part of the load-bearing frame? Do the hydrates fill the pores of the sediments without affecting the mineral frame? Are the hydrates layered bodies? Do the hydrates occur as nodules and veins?

In this report, we present rock physics models for unconsolidated sediments in which hydrates are assumed to be present in the following geometrical occurrences: *a*) disseminated, load-bearing clathrates that are part of the mineral frame of the host sediments; *b*) pore-filling clathrates that float in the porous space without changing the dry mineral frame of the host sediments; *c*) thin layers of horizontal or vertical hydrates intercalated with thin layers of hydrate-free sediments saturated with fluid; and *d*) thin layers of disseminated, load-bearing hydrates intercalated with thin layers of hydrate-free sediments saturated with fluid.

Our objective is to understand the relationships between hydrate concentrations and V_P and V_S seismic velocities for these four scenarios of possible hydrate-sediment morphology. We also simulate seismic amplitude variation with angle of incidence (AVA) for P-P and P-SV reflectivity at a hypothetical interface separating the base of the hydrate stability zone and deeper sediments that contain free gas. For aligned vertical layers of pure hydrate, we model amplitude variation with incidence angle and azimuth because this type of medium has azimuthal variablity. We emphasize the importance of analyzing azimuthal variations of the seismic amplitudes to identify and quantify this type of hydrate distribution. We show that the geometrical details of how gas hydrates are distributed within sediments have a significant impact on the relationships between hydrate concentration and seismic velocities. This research finding shows that to produce estimates of hydrate concentrations from seismic data, we need to understand how hydrates are distributed within their host sediments. Our modeling results for the two thin-layered hydrate/sediment morphologies (cases c and d listed above) show significant S-wave anisotropies. These S-wave-splitting effects can be used to infer hydrate distribution and concentration in near-seafloor environments that have alternating thin layers of hydrate-bearing and hydrate-free sediments if multicomponent seismic data are acquired across targeted hydrate systems.

We compare the theoretical predictions of V_P and V_S velocity behavior from our rock-physics models with laboratory measurements by Yun et al. (2005) on synthetic, load-bearing hydrates formed in unconsolidated sands and clays. We find good agreement between our rock physics model of disseminated, load-bearing hydrates (morphology option "a" listed above) and these laboratory measurements. This observation suggests that our rock physics theory is correctly structured.

Experimental

Experimental work in Task 8 consisted of the development of rock physics theory and the conversion of this theory into functioning software code.

Results and Discussion

Rock Physics Model for Unconsolidated Sediments

The elastic properties of marine hydrate systems depend on the elastic properties of their host sediments. We first present the background and theoretical aspects of rock physics modeling of the elastic properties of unconsolidated marine sediments found in near-seafloor, deep-water environments. We then summarize a practical methodology for estimating these elastic properties.

Background and Theory

Newly deposited sediments at the bottom of the ocean are in a pseudo-suspension regime and their shear strength is almost zero near the seafloor. The V_P/V_S velocity ratio is large within the first few meters of sediment and tends to infinity at the boundary between ocean-bottom sediments and the water column.

Most rock physics models for unconsolidated sediments are based on contact models, such as Hertz-Mindlin's theory (Mindlin, 1949), for describing the elastic properties of granular materials. The porosity at which a granular composite ceases to be a suspension and becomes grain-supported is called the **critical porosity**. Dvorkin and Nur (1996) assume that at critical porosity the effective elastic moduli of the dry-mineral frame of sediments can be calculated using Hertz-Mindlin's contact theory for elastic particles. For porosity values smaller than critical porosity, the elastic properties of the dry-mineral frame are estimated using the modified **Hashin-Shtrikman Lower Bound** (1963). For porosity values larger than critical porosity, Dvorkin et al. (1999) propose to use a modified **Hashin-Shtrikman Upper Bound** to derive the elastic properties of the dry-mineral frame of granular materials. Gassmann's (1951) theory is then used to derive the elastic properties of the sediments saturated with fluids. These modeling assumptions have been applied to marine sediments (Prasad and Dvorkin, 2001) in various areas around the globe. However, Hertz-Mindlin's theory is not appropriate for sediments within the first 100 or 200 meters below the seafloor where S-wave velocity is quite small, and implicitly the V_P/V_S ratio is large, as in-situ observations from four-component ocean-bottom-cable (4C-OBC) data suggest (Backus et al, 2006; Hardage et al., 2007). For this type of environment, Hertz-Mindlin theory will predict V_S velocities that are too high. S-wave velocities have also been observed in laboratory measurements on unconsolidated sediments (e.g. Zimmer, 2003; Yun et. al, 2005) which are significantly lower than V_S values predicted by Hertz-Mindlin's theory. The main reason for the discrepancy between S-wave velocity measurements and theory is that the Hertz-Mindlin model overestimates the shear modulus for granular composites.

Hertz-Mindlin theory assumes infinite friction at grain contacts and does not allow grain rotation and slip at grain boundaries, which are physical processes that occur between unconsolidated grains, especially at low effective pressures encountered near the seafloor. We propose a new model that is based on the initial approach of Dvorkin and Nur (1996) and Dvorkin et al. (1999), but we use the distinction that at critical porosity the elastic properties of deep-water, near-seafloor sediments are described by Walton's (1987) contact theory, not by Hertz-Mindlin theory. Walton's model, like other contact models (Digby, 1981; Mavko et al., 1998), assumes that the granular material is made up of an aggregate of perfect spheres.

Hertz-Mindlin Theory

To illustrate the difference between the Hertz-Mindlin and Walton models, we note that the elastic moduli of such a granular material derived using Hertz and Mindlin's solutions for the displacement of two identical spheres in contact under normal and shear forces are (Mavko et al, 1998):

$$K_{eff} = \frac{C(1-\phi)}{12\pi R} S_n, \qquad G_{eff} = \frac{C(1-\phi)}{20\pi R}\left(S_n + 1.5 S_\tau\right). \tag{1}$$

K_{eff} and G_{eff} are the effective **bulk** and **shear moduli**, respectively, for the granular material. C is the **coordination number**, which represents the average number of contacts between a grain and its neighboring grains. Φ is the **porosity** of the aggregate of spheres, and R is the **radius** of the identical spheres representing the grains. S_n and S_τ are the **normal** and **tangential stiffnesses**, respectively, of two grains in contact and depend on effective pressure, radius of contact of the two grains, and elastic bulk and shear moduli of the grain mineral. In terms of effective pressure, the standard Hertz-Mindlin's expressions for the effective bulk and shear moduli are:

$$K_{eff} = \sqrt[3]{\frac{C^2(1-\phi)^2 G^2}{18\pi^2(1-\nu)^2} P}, \qquad G_{eff} = \frac{5-4\nu}{5(2-\nu)} \sqrt[3]{\frac{3C^2(1-\phi)^2 G^2}{2\pi^2(1-\nu)^2} P}. \tag{2}$$

G and ν are the **shear modulus** and the **Poisson's ratio**, respectively, for the mineral grains, and P is the **effective pressure**.

Walton Model

Walton (1987) derived a model that assumes there is no friction between contacting grains, referred to as a "**smooth model**". The physical meaning of this model is that grains are allowed to rotate and slip at their contact boundaries. This assumption

reduces the effective shear strength of a granular material in comparison with the Hertz-Mindlin's assumption that there is infinite friction between the grains. Mathematically, Walton's model sets the tangential stiffness (S_τ) between two grains in contact to zero in the standard Hertz-Mindlin's expressions in Equation 1, which causes the effective shear modulus (G_{eff}) to be reduced to 60-percent of the bulk modulus. The expressions for the bulk and shear moduli for a random arrangement of dry spheres using Walton's approach are:

$$K_{eff} = \sqrt[3]{\frac{C^2(1-\phi)^2 G^2}{18\pi^2(1-\upsilon)^2} P},$$
$$G_{eff} = \frac{3}{5} K_{eff}. \quad (3)$$

If we compare Equations 2 and 3, we observe that the effective shear modulus for Walton's smooth model is smaller than that of Hertz-Mindlin's model, and the ratio between the two shear moduli is the following simple function of the Poisson's ratio of the grain mineral:

$$G_{eff}^{Walton} = \frac{2-\nu}{5-4\nu} G_{eff}^{Hertz-Mindlin} . \quad (4)$$

In the case of quartz grains that have a Poisson's ratio of 0.08 (Mavko et al. 1998), the effective shear modulus given by Walton's expression is only 41 percent of the effective shear modulus predicted by Hertz-Mindlin's theory. Therefore, Walton's model predicts a shear velocity that is approximately 0.64 of the shear velocity predicted by Hertz-Mindlin's model for granular materials with quartz grains.

Walton's model is particularly appropriate for unconsolidated sediments at low effective pressure where grain rotation and slip along grain boundaries are most likely to occur. Walton's model better explains the low shear strengths and high V_P/V_S ratios observed in 4C OBC seismic data acquired across deep-water, near-seafloor strata, as well as laboratory measurements made on unconsolidated sediments.

Methodology

We calculate the elastic properties of unconsolidated deep-water granular materials over a large porosity range using the following five steps:

1. Compute the bulk and shear moduli of the dry mineral frame at *critical porosity* using Walton's theory (Equation 3). If the solid grains are a mixed mineralogy, then the bulk modulus and shear modulus (*K* and *G*) of the composite material can be computed from the moduli of the individual mineral constituents using Hill's (1963) average defined as:

$$K = \frac{1}{2}\left[\sum_{i=1}^{m} f_i K_i + \left(\sum_{i=1}^{m} \frac{f_i}{K_i}\right)^{-1}\right],$$
$$G = \frac{1}{2}\left[\sum_{i=1}^{m} f_i G_i + \left(\sum_{i=1}^{m} \frac{f_i}{G_i}\right)^{-1}\right]. \quad (5)$$

In this equation, ***m*** is the number of mineral constituents for the solid phase, f_i is the volumetric fraction of the i^{th} constituent, and K_i and G_i are the bulk and shear moduli, respectively, of the i^{th} mineral constituent.

2. Derive the elastic moduli of the dry frame for porosity values Φ smaller than critical porosity Φ_c, using the modified Hashin-Shtrikman Lower Bound, as follows:

$$K_{dry} = \left(\frac{\phi/\phi_c}{K^{Walton} + \frac{4}{3}G^{Walton}} + \frac{1-\phi/\phi_c}{K + \frac{4}{3}G^{Walton}}\right)^{-1} - \frac{4}{3}G^{Walton},$$
$$G_{dry} = \left(\frac{\phi/\phi_c}{G^{Walton} + Z} + \frac{1-\phi/\phi_c}{G + Z}\right)^{-1} - Z, \quad (6)$$

where

$$Z = \frac{G^{Walton}}{6}\left(\frac{9K^{Walton} + 8G^{Walton}}{K^{Walton} + 2G^{Walton}}\right). \quad (7)$$

Moduli K_{dry} and G_{dry} from Equation 6 correspond to the weakest possible option for combining the solid phase (which has moduli K and G) and the critical-porosity material [which has moduli given by Walton's theory (K^{Walton} and G^{Walton})].

3. Derive the elastic moduli of the dry frame for porosity values Φ larger than the critical porosity Φ_c using a modified Hashin-Shtrikman Upper Bound by combining the critical-porosity material and the void space, the latter having zero bulk or shear strength:

$$K_{dry} = \left(\frac{(1-\phi)/(1-\phi_c)}{K^{Walton} + \frac{4}{3}G^{Walton}} + \frac{(\phi-\phi_c)/(1-\phi_c)}{\frac{4}{3}G^{Walton}}\right)^{-1} - \frac{4}{3}G^{Walton},$$
$$G_{dry} = \left(\frac{(1-\phi)/(1-\phi_c)}{G^{Walton} + Z} + \frac{(\phi-\phi_c)/(1-\phi_c)}{Z}\right)^{-1} - Z. \quad (8)$$

Moduli K_{dry} and G_{dry} from Equation 8 correspond to the stiffest possible combination of critical-porosity material and void space.

4. Compute the elastic moduli for the unconsolidated granular material saturated with fluid using Gassmann's (1951) equation:

$$K_{sat} = K\frac{\phi K_{dry} - (1+\phi)K_{fl}K_{dry}/K + K_{fl}}{(1-\phi)K_{fl} + \phi K - K_{fl}K_{dry}/K},$$
$$G_{sat} = G_{dry}. \qquad (9)$$

In Equation 9, K_{sat} represents the bulk modulus of the fluid-saturated granular material. G_{sat} is the shear modulus for the fluid-saturated sediment, which is the same as the shear modulus G_{dry} for the dry granular material. K_{fl} is the bulk modulus of the fluid, K_{dry} is the effective bulk modulus of the dry frame, and K is the bulk modulus of the solid grains.

5. Compute the bulk density of the unconsolidated sediments, which is given by:

$$\rho = \phi\rho_{fl} + (1-\phi)\rho_{grain},$$

with
$$\rho_{grain} = \sum_{i=1}^{m} f_t \rho_i \ . \qquad (10)$$

In Equation 10, ρ is the bulk density of the fluid-saturated sediments, ρ_{fl} is the density of the saturating fluid, and ρ_{grain} is the density of the solid phase. In a case of mixed mineralogy, the density of the solid phase (ρ_{grain}) is given by the volumetric average of the densities of the individual constituents. In the above equation, m is the number of mineral constituents for the solid phase, f_i is the volumetric fraction of the i^{th} constituent, and ρ_i is the density of the i^{th} mineral constituent.

If we assume an isotropic medium, then the bulk modulus and shear modulus (Equations 9) together with density (Equations 10) completely characterize the elastic properties of unconsolidated, fluid-saturated sediments over the full porosity range of deep-water sediments. From these three quantities (K, G, ρ), we derive the P- and S-wave velocities of the unconsolidated sediments. Based on the methodology summarized in steps 1 to 5, we proceed to develop rock-physics models for unconsolidated sediments in deep-water, near-seafloor strata that contain hydrates.

Rock Physics Models for Hydrate Systems

The effective elastic properties of hydrate systems depend on: 1) the elastic properties of the host sediments, 2) the elastic properties of pure hydrates, 3) hydrate concentration, and 4) the geometrical details of how the hydrates are distributed within the sediments. We have analyzed models of hydrate systems that can occur in the low-

effective-pressure zone that spans the first 200 or 300 meters of sub-seafloor strata. We based our rock physics modeling of deep-water hydrate systems on the mathematical development of the elastic properties of unconsolidated sediments that are presented in the previous section. Specifically, we considered the following four rock physics models for marine hydrate systems (Figure 1):

- **Model A** assumes hydrates are uniformly disseminated throughout the sediment and are part of the load-bearing frame of the host sediments.
- **Model B** assumes hydrates are also disseminated throughout the sediment, but they only float in the porous space and do not change the dry mineral frame of their host sediments.
- **Model C** assumes an anisotropic, thin-layered medium in which layers of pure gas hydrate are intercalated with layers of hydrate-free sediments saturated with fluid. These thin layers can be horizontal or vertical. Vertical thin layers approximate thin fractures and veins filled with pure hydrate.
- **Model D** is also an anisotropic, thin-layered medium. However, in this model, hydrates are disseminated in thin layers of sediments in which they occupy 99-percent of the porous space and are part of the load-bearing frame. These thin hydrate-bearing layers are intercalated with thin layers of hydrate-free sediments saturated with fluid.

The key input parameter in all of these models is hydrate concentration. Our goal is to quantitatively relate hydrate concentration to seismic P- and S-wave velocities and to amplitude variation with angle of incidence (AVA) for each of these hydrate-sediment morphologies.

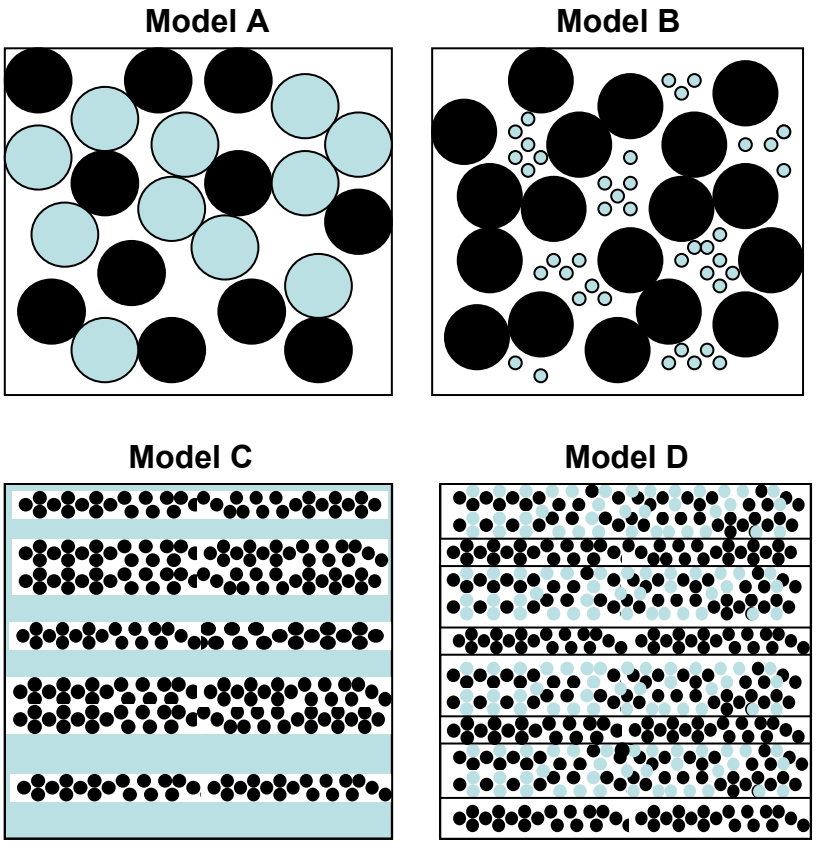

Figure 1: Graphical sketch of the four models of marine hydrate systems: load-bearing hydrates (Model A); pore-filling hydrates (Model B); thin layers of horizontal or vertical pure hydrate intercalated with unconsolidated hydrate-free sediments (Model C); thin layers of disseminated, load-bearing hydrates intercalated with unconsolidated, hydrate-free sediments (Model D). Hydrates are represented in light blue and sediment in black.

Model A: Hydrates as Part of the Load-Bearing Frame

In this model we assume that hydrates are disseminated throughout the volume of sediments and are a part of the load-bearing frame, a concept proposed by Helgerud et al. (1999). We start with the rock physics model for unconsolidated granular materials presented as Equations 1 through 10. Then we derive the effective elastic properties of sediments containing different concentrations of hydrate by incorporating the hydrate phase into the mineral frame (Helgerud et al., 1999) and by reducing accordingly the initial porosity of the host sediments. When hydrate is present, the initial porosity Φ of the unconsolidated sediments without hydrates reduces to an effective porosity Φ_{eff} given by:

$$\phi_{eff} = \phi - c_{gh}, \tag{11}$$

where c_{gh} represents the volumetric hydrate concentration in the unconsolidated rock. When we incorporate hydrates into the system, the porosity (Φ) of our base model for

unconsolidated sediments without hydrate is replaced in Equations 6, 8, 9 and 10 by the effective porosity defined in Equation 11.

When hydrate is considered to be part of the mineral frame, its volumetric fraction within the solid phase, f_{gh}, is given as:

$$f_{gh} = \frac{c_{gh}}{1-\phi_{eff}}. \tag{12}$$

The volumetric fractions of the other mineral phases change accordingly as,

$$f_i^{eff} = \frac{1-\phi}{1-\phi_{eff}}. \tag{13}$$

These new volumetric fractions for the mineral phases (f_i^{eff}) and for the gas hydrates (f_{gh}) replace the original volumetric fractions (f_i) in Equations 5 and 10 for the model of unconsolidated sediments without gas hydrates. In this way, we compute the new bulk modulus, shear modulus, and density of the dry mineral frame containing hydrates with concentration c_{gh}.

Using Equations 11, 12 and 13 together with the model for unconsolidated sediments presented in the previous section, we compute the elastic properties of sediments with disseminated, load-bearing hydrates in different concentrations.

Model B: Hydrates as Pore-Filling Clathrates

In this model, we assume that hydrates are distributed in the porous space, but they do not alter the dry mineral-frame of the sediments, (Helgerud et al., 1999). This model implies that the hydrates are floating in the pores, away from the grains, and their effect is to modify only the elastic properties of the material filling the sediment pores without affecting the shear-strength of the host sediments.

We assume the small unit volumes of hydrates are suspended in the fluid that saturates the pores. The elastic properties of the pore-filling material (a mixture of hydrate clathrates and fluid) are given by Reuss (1929) averaging, implying this mixture does not have any shear strength. The bulk modulus of the mixture of hydrate clathrates suspended in fluid is:

$$K_{gh\_fluid} = \left[\frac{f_{gh}}{K_{gh}} + \frac{f_{fluid}}{K_{fluid}} \right]^{-1}. \tag{14}$$

In this equation, K_{gh_fluid} is the bulk modulus of the mixture of hydrates and fluid in the porous space, f_{gh} represents the fraction of hydrates that occupies the porous space (which varies from *0* to *1*) and $f_{fluid}=1-f_{gh}$ is the fraction of fluid that occupies the porous space.

The volumetric gas-hydrate concentration, c_{gh}, in the whole volume of sediments is related to the volumetric fraction of gas hydrates in the pores (f_{gh}) and is given by,

$$c_{gh} = \Phi f_{gh}, \quad (15)$$

where Φ is the porosity of the host sediments.

To summarize our model calculations, we start with the rock physics model for unconsolidated sediments presented as Equations 1 through 10. Initially, these sediments with porosity Φ are saturated with fluid. Next we predict the elastic properties of the sediments with hydrates in the pores using Gassmann's (1951) theory. The bulk modulus of the mixture of hydrates and fluid (K_{gh_fluid}) from Equation 14 then replaces the fluid bulk modulus (K_f) from Equation 9 in the original model for unconsolidated sediments without hydrates.

This model predicts the shear strength of sediments with pore-filling hydrates is the same as the shear strength of sediments that are 100-percent saturated with fluid. Therefore, the shear modulus of sediments with pore-filling hydrates is the same as the shear modulus of the unconsolidated sediments in Equation 9. However, Gassmann (1951) theory predicts the bulk modulus of the sediments with pore-filling hydrates will increase as hydrate concentration increases.

The bulk density of the sediment changes when hydrates replace part of the fluid in the porous space because the densities of fluid and hydrates are different. The adjusted bulk density is given by:

$$\rho = \left[f_{gh}\rho_{gh} + (1 - f_{gh})\rho_{fl} \right]\phi + (1 - \phi)\rho_{grain} \quad (16)$$

In this equation, ρ is the bulk density of the sediments with pore-filling hydrates, ρ_{gh} is the density of the hydrates, f_{gh} is the fraction of hydrates that replaces the fluid in the pores, ρ_{fl} is the density of the fluid, Φ is the porosity of the unconsolidated sediments, and ρ_{grain} is the density of the mixture of mineral grains (Equation 10).

Model C: Thin-Layered Model with Pure Hydrates

Our third model is represented by a layered medium made up of thin beds of pure gas hydrates intercalated with unconsolidated hydrate-free sediments. Backus (1962) showed that in the long-wavelength limit, a stratified medium with individual isotropic layers is effectively anisotropic. If the thin layers are horizontal, this type of anisotropy is transversely isotropic with a vertical axis of symmetry (VTI medium). The anisotropic effective elastic properties of such a thin-layered medium depend on the elastic properties of the individual layered materials and their volumetric proportions in the rock (Backus, 1962).

In our case, the stratified medium is composed of two different materials: pure hydrate and unconsolidated marine sediments saturated with fluid. The elastic properties of pure hydrate are known (Sloan, 1998), and the elastic properties of unconsolidated sediments saturated with fluid can be estimated from the rock physics model presented in Equations 1 through 10. Therefore, using Backus averaging, we predict the elastic stiffness matrix for a layered medium having different hydrate concentrations. The volumetric concentration of hydrate (c_{gh}) for the whole volume of

sediments is equal to the volumetric fraction (f_{gh}) of hydrate layers in the stratified medium:

$$c_{gh} = f_{gh.} \tag{17}$$

Because this model describes an anisotropic medium, the effective elastic properties will vary with direction. In particular, S-waves polarized perpendicular to the layers (slow direction) will propagate with a slower velocity than S-waves polarized parallel to the layers (fast direction). Also, P-waves propagating orthogonal to the layers will have slower velocity than the P-waves propagating along the layers.

The bulk density of the anisotropic thin-layered model is given by volumetric averaging of the densities of the two constituent materials: hydrate (ρ_{gh}) and unconsolidated sediments saturated with fluid (ρ, from Equation 10).

If the layers are vertical instead of horizontal, we can still use Backus averaging to estimate the effective anisotropic elastic properties of such a medium, but we need to apply a rotation to the elastic stiffness matrix to obtain a transversely isotropic medium with a horizontal axis of symmetry (HTI medium). This model of thin vertical layers approximates thin, vertical, aligned fractures/veins or vertical dykes filled with hydrate. The main difference between HTI and VTI media is that an HTI medium generates an azimuthally anisotropic medium, but a VTI medium does not.

Model D: Thin-Layered Model with Disseminated Hydrates

The last model we consider is another thin-layered medium, with layers of hydrate disseminated in unconsolidated sediments. The hydrate in these layers is assumed to be part of the load-bearing frame and to occupy a certain fraction (f_{gh}) of the porous space of the host sediment. Layers containing hydrates are intercalated with layers of unconsolidated sediments that are 100-percent saturated with fluid. The elastic properties of the layers containing hydrates are estimated using Model A; whereas, the elastic properties of the unconsolidated sediments saturated with fluid are estimated using the rock physics model presented as Equations 1 through 10. In the assumption that the medium is thinly-bedded, we again use Backus (1962) averaging to determine the elastic properties of the layered sediments for different hydrate concentrations. The overall volumetric concentration of hydrate in the rock is given by,

$$C_{gh} = f_{lr} f_{gh} \Phi. \tag{18}$$

In this equation, f_{lr} represents the volumetric fraction of layers containing disseminated hydrates, f_{gh} represents the proportion of hydrates occupying the porous space of these layers, and Φ is the porosity of the layers containing hydrates. For this model, we assume hydrates occupy 99-percent of the porous space ($f_{gh} = 0.99$). This model is also anisotropic, and P- and S-wave velocities will vary with direction, as they do for layered model C.

The bulk density of the thinly bedded medium is given by volumetric averaging of the densities of the two constituent materials: the sediments with load-bearing hydrates (see Model A) and the unconsolidated sediments saturated with fluid (Equation 10).

Results

In this section we present P- and S-wave velocities predicted by the four different rock physics models of hydrate systems described in the previous section. The rock-property parameters used in the modeling are summarized in the following table.

Constituent	Bulk Modulus	Shear Modulus	Density
quartz	37 GPa	44 GPa	2650 kg/m3
clay	25 GPa	9 GPa	2550 kg/m3
brine	2.29 GPa	0 GPa	1005 kg/m3
gas hydrate	7.14 GPa	2.4 GPa	910 kg/m3

Pure-Quartz Host Sediment

In the examples from Figures 2, 3, and 4, we consider the unconsolidated sediments to be represented by pure quartz grains saturated with brine. The sediments are assumed to be at critical porosity of 37 percent. The coordination number *C* is considered to be 8, and the effective pressure is set at a low value of 0.01 MPa. This low value of effective pressure corresponds to a depth of approximately 2 meters below the seafloor. This low effective-pressure value can also correspond to deeper strata within overpressured zones, which may be encountered in the Gulf of Mexico.

Figures 2, 3, and 4 present the modeling results for P-wave velocity (V_P), S-wave velocity (V_S), and V_P/V_S ratio, respectively, as a function of hydrate concentration (c_{gh}) for the four rock physics models A, B, C and D. For the two anisotropic layered models (C and D), we display two curves corresponding to velocity of waves with their particle-displacement vector parallel to the layering (solid line) and to velocity of waves with their particle displacement vector orthogonal to the layers (dotted lines). From all of these figures we can observe that P- and S-wave velocities depend on the geometrical details of how gas hydrates are distributed in their host sediments.

The results presented in Figure 2 show that for these four rock physics models, the presence of hydrate increases the P-wave velocity in the sediments. The smallest increase in P-wave velocity with hydrate concentration is obtained for the thin-bedded model with layers of pure hydrates (Model C), while the largest increase in P-wave velocity is obtained for the models having disseminated, load-bearing hydrates (Models A and D). The rate of change of V_P with hydrate concentration is greatest when measured parallel to the thin layers of load-bearing clathrates (Model D).

If we consider the two thin-layered models (Models C and D), we see that the fast P-wave velocity propagating parallel to the layers (solid lines) and the slow P-wave velocity propagating orthogonal to the layers (dotted lines) are different for these two morphologies (Figure 2). For example, at a 0.3 volumetric concentration of hydrate, fast P-wave velocity can range from 2000 m/s for layers of pure hydrates (Model C, solid line) to more than 3000 m/s for layers of disseminated, load-bearing hydrates (Model D, solid line). This large difference in V_P is caused partly because the elastic moduli of layers having load-bearing hydrates are larger than the elastic moduli of pure hydrates.

In addition, the volumetric fraction of layers having disseminated hydrates is 2.73 [$(0.99\Phi)^{-1}$] times larger than the corresponding fraction of layers of pure hydrates for the same volumetric hydrate concentration in the two layered media. This value of 2.73 is obtained by comparing Equations 17 and 18, and setting Φ, the porosity of the unconsolidated sediments, to a value of 0.37, a common value for the critical porosity of round, uniform-size grains. When the volumetric fraction for the layers of disseminated hydrates in the thin-bedded medium is 1, the rock becomes isotropic, and the end points of the two curves for Model D coincide with the end point of the curve for Model A (Figure 2).

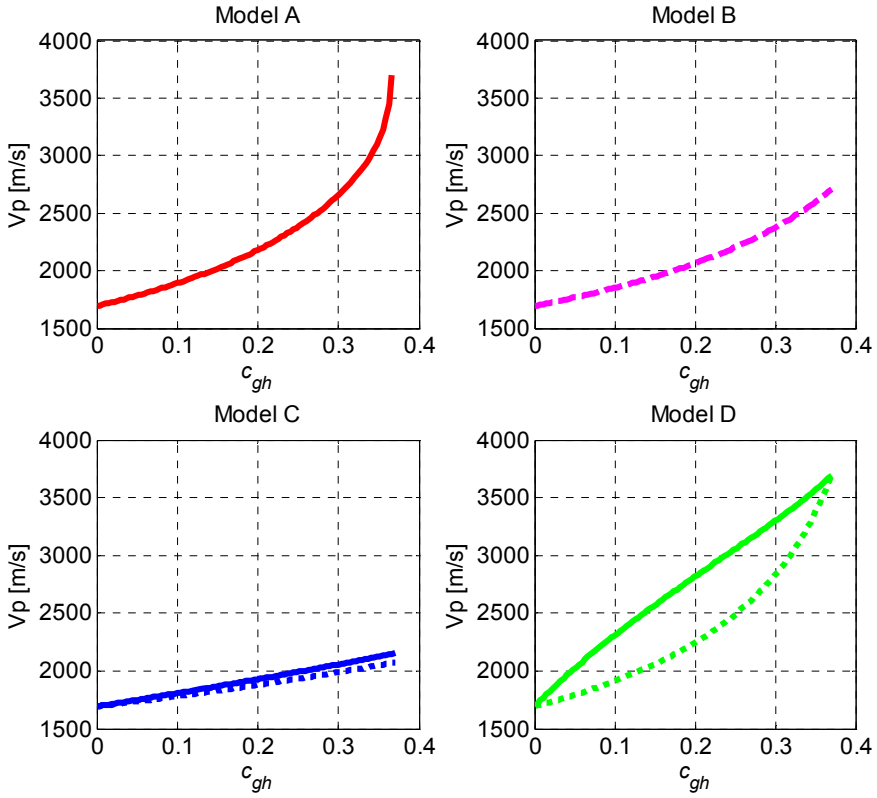

Figure 2: P-wave velocity as a function of the volumetric fraction of hydrate (c_{gh}) in pure quartz sediments for the four rock physics models. **Model A**: load-bearing hydrates disseminated in the sediments; **Model B**: pore-filling hydrates disseminated in the sediments; **Model C**: horizontal or vertical layers of pure hydrates producing slow P-waves (dotted line) and fast P-waves (solid line); **Model D**: layers of disseminated, load-bearing hydrates producing slow P-waves (dotted line) and fast P-waves (solid line). C_{gh} is shown as a fraction of the unit volume. All curves terminate at critical porosity, 0.37.

From Figure 3 we observe that S-wave velocity also increases with hydrate concentration for all four rock physics models. However, for the model in which the hydrate floats in the porous space without contributing to the load-bearing frame of the host sediments (Model B), the increase in S-wave velocity is insignificant. In this model the hydrates are not connected to the mineral frame, and even though the hydrate unit volumes are solid, they do not support any shear load. Gassmann's (1951) theory used in this model predicts that the shear modulus of the sediments does not change with hydrate concentration. Because there is only a minor difference in the densities of brine

and hydrate, there is only a small increase in V_S when gas hydrate replaces brine in the pores.

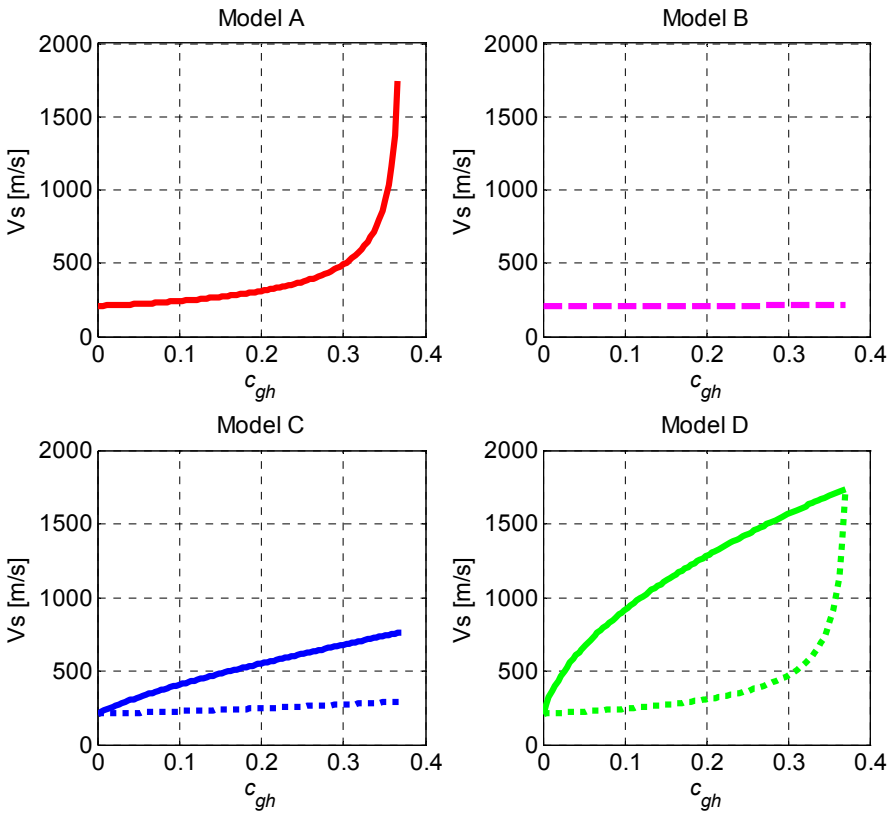

Figure 3: S-wave velocity as a function of the volumetric fraction of hydrate (c_{gh}) in pure quartz sediments for the four rock-physics models. **Model A**: load-bearing hydrates disseminated in the sediments; **Model B**: pore-filling hydrates disseminated in sediments; **Model C**: horizontal or vertical layers of pure hydrates producing S-waves with slow polarization (dotted line) and fast polarization (solid line); **Model D**: layers of disseminated, load-bearing hydrates producing S-waves with slow polarization (dotted line) and fast polarization (solid line). C_{gh} is shown as a fraction of the unit volume. All curves terminate at critical porosity, 0.37.

The results presented in Figure 3 show a large increase in S-wave velocity occurs when the waves are polarized parallel to the layers of a medium having thin beds of disseminated, load-bearing hydrates (Model D, solid line). In this particular type of hydrate/sediment morphology, the velocity of S-waves propagating with their displacement vector polarized parallel to the layering (fast direction) increases significantly for small hydrate concentrations. This behavior suggests that for disseminated, load-bearing hydrates occurring in thin beds, we may be able to detect small hydrate concentrations using anisotropic S-wave information. The S-wave anisotropy for this model is large. There is a large difference between S-wave velocities polarized parallel (Model D, solid line) and orthogonal (Model D, dotted line) to layers of disseminated, load-bearing hydrates. S-wave anisotropy for a system of layers of pure hydrates (Model C) is large as well. Therefore, if hydrates occur in thin layers within near-seafloor strata, we should expect significant shear-wave anisotropy, and this anisotropy may be used with other seismic information to estimate hydrate

concentrations. If the medium exhibits thin vertical layers of pure hydrate (approximating aligned, vertical thin fractures/veins filled with hydrates), we should expect not only shear-wave splitting, but also azimuthal anisotropy in both wave velocities and reflectivities. These anisotropic seismic attributes can be excellent indicators for quantifying hydrate distribution and concentration.

For Model A, S-wave velocity increases little at small hydrate concentrations, then increases abruptly at hydrate concentrations larger than 0.3 (i.e. when load-bearing clathrates occupy more than 80-percent of the pore volume). Thus, it will be more challenging to determine small hydrate concentrations using S-wave information when load-bearing clathrates are uniformly disseminated within the sediments. Note again that the end points of the curves for Model A and Model D coincide, as they should.

Figure 4 presents the V_P/V_S ratio for the four rock-physics models. This velocity ratio decreases with hydrate concentration for all models except Model B that assumes pore-filling hydrates. This anomalous behavior for Model B occurs because P-wave velocity increases with hydrate concentration (Figure 2) while S-wave velocity remains practically constant (Figure 3). As a result, the V_P/V_S velocity ratio for Model B increases with hydrate concentration.

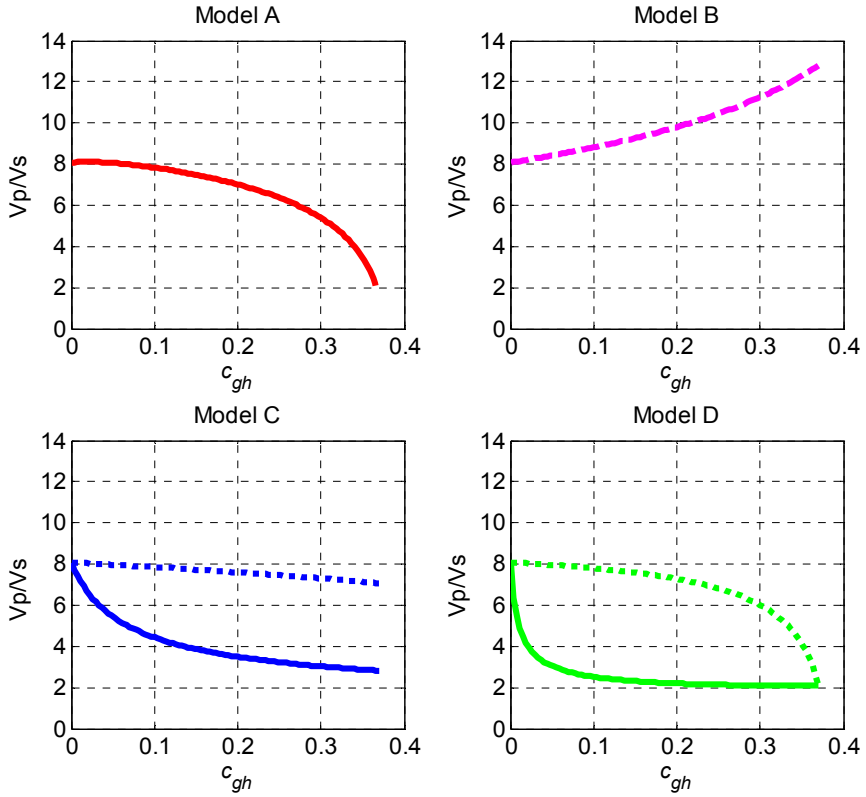

Figure 4: Vp/Vs ratio as a function of the volumetric fraction of hydrate (c_{gh}) in pure quartz sediments. **Model A**: load-bearing hydrates disseminated in the sediments; **Model B**: pore-filling hydrates disseminated in the sediments; **Model C**: horizontal or vertical layers of pure hydrates producing slow waves (dotted line) and fast waves (solid line); **Model D**: layers of disseminated, load-bearing hydrates producing slow waves (dotted line) and fast waves (solid line). C_{gh} is shown as a fraction of the unit volume. All curves terminate at critical porosity, 0.37.

From Figure 4 we observe that the V_P/V_S velocity ratio for slow P and S-waves polarized orthogonal to layers of disseminated, load-bearing gas hydrates (Model D, dotted line) is similar to the V_P/V_S ratio when load-bearing hydrates are uniformly disseminated in the sediments (Model A). For these two models, the velocity ratio decreases slightly at small hydrate concentrations and more abruptly for larger hydrate concentrations. This behavior suggests it will be challenging to estimate small hydrate concentrations using V_P/V_S ratios in media represented by either of these curves. However, for anisotropic Models C and D, there is a significant decrease in the V_P/V_S ratio at low hydrate concentration for waves with particle-displacement vectors parallel to the layers (fast direction, solid curve). This modeling result suggests that for layered hydrate morphologies, we may be able to use V_P/V_S ratios and anisotropy information to detect small hydrate concentrations in sediments.

Mixed-Mineralogy Host Sediment

The theory presented in the preceding sections allows for mixed mineralogy, as well as for different saturating fluids. Figures 5, 6, and 7 are similar to Figures 2, 3, and 4, respectively, except that the curves displayed in each panel correspond to different clay and sand mixtures. The clay content in the sediments varies from 0 to 100 percent, at a 25-percent increment. Some parameters used in the modeling, such as critical porosity and coordination number, vary with mineralogy (Murphy, 1982). For clean quartz grains (0 percent clay content), the critical porosity is assumed to be 37 percent, and the coordination number C is considered to be 8. For pure clay minerals (100-percent clay content), we use a larger critical porosity of 67 percent and a smaller coordination number of 4, as many geotechnical data suggest (Murphy, 1982). For each mixture of quartz and clay minerals, we derive the values for critical porosity and coordination number by doing a linear interpolation between the corresponding values for the two end members of pure quartz and pure clay. Also, at sub-seafloor depths where hydrates are stable, the porosity of clay-rich sediments is larger than the porosity of pure quartz grains. Therefore, we compute V_P and V_S as a function of hydrate concentration for sediments with different porosity values: 37 percent for pure quartz and 50 percent for pure clay minerals. For each mixture of quartz and clay, we use again a linear interpolation between the values for the two end members of pure quartz and pure clay. The effective pressure we use in these calculations is equal to 0.5 MPa, which corresponds to a depth below seafloor of approximately 60 m.

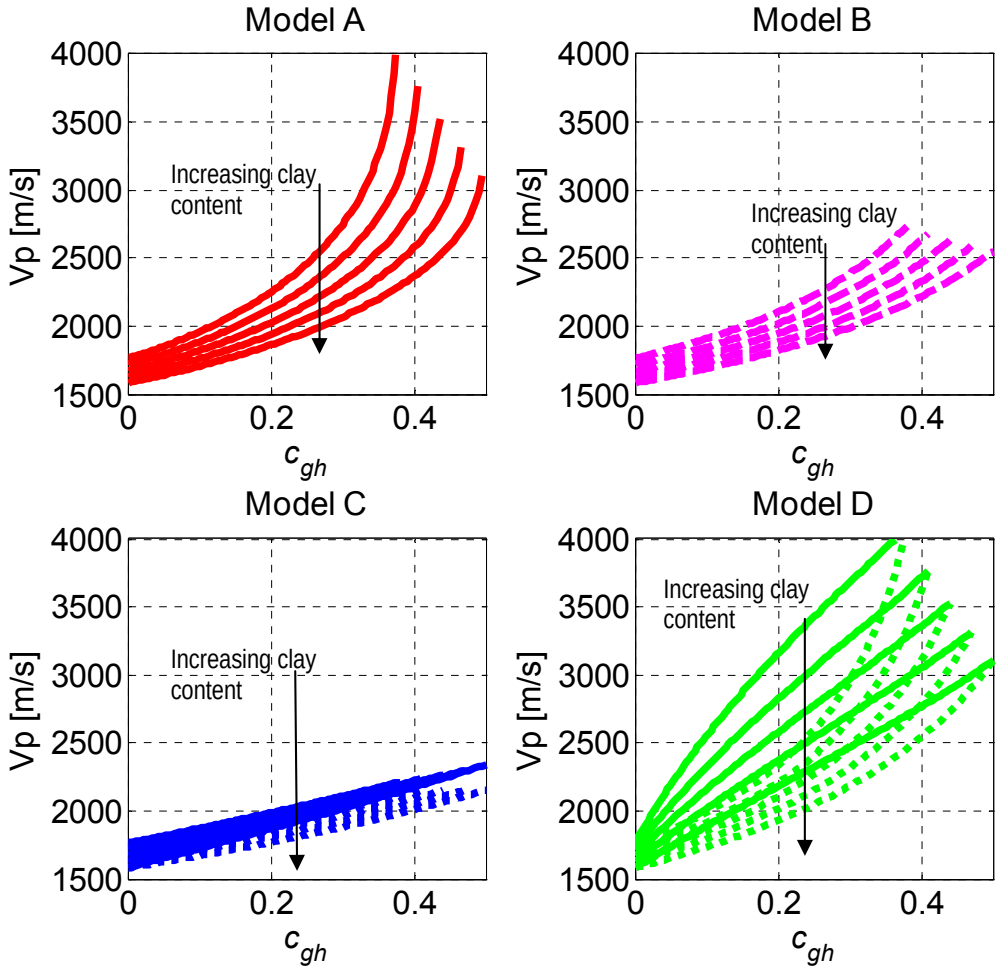

Figure 5: P-wave velocity as a function of the volumetric fraction of hydrate (c_{gh}) in a sediment mixture with variable clay content. **Model A**: load-bearing hydrates disseminated in the sediments; **Model B**: pore-filling hydrates disseminated in the sediments; **Model C**: horizontal or vertical layers of pure hydrates producing slow P-waves (dotted lines) and fast P-waves (solid lines); **Model D**: layers of disseminated, load-bearing hydrates producing slow P-waves (dotted lines) and fast P-waves (solid lines). Each curve corresponds to a different clay content (ranging from 0 to 100 percent at a 25-percent increment), different critical porosity values, and different coordination numbers. The curves are computed at increasing porosity values as the clay content increases. The arrows indicate increasing clay content.

As expected, the P- and S-wave velocities decrease with increasing clay content (and implicitly with increasing porosity), as we observe from each panel in Figures 5 and 6. For Model A (load-bearing hydrates), as porosity and clay content of the sediments increase, it becomes more challenging to estimate small hydrate concentrations, especially using S-wave velocity data. For layered model D, we observe that both P- and S-wave anisotropy decreases with increasing clay content because the elastic properties of clay minerals are closer to those of hydrates than are the elastic properties of quartz minerals. This modeling shows that we should expect larger anisotropy in P- and S-wave velocities if hydrate layers are intercalated with clean sands than with clay-

rich sediments. Models D and C take into account only the anisotropy due to thin layers and consider the clay-rich sediments to be isotropic. This assumption may hold for sediments immediately below seafloor. However, as depth increases, the stress-induced anisotropy of clays is going to increase. At large depths, Models C and D with clay-rich sediments should be adjusted to account for anisotropy caused by the presence of clay minerals.

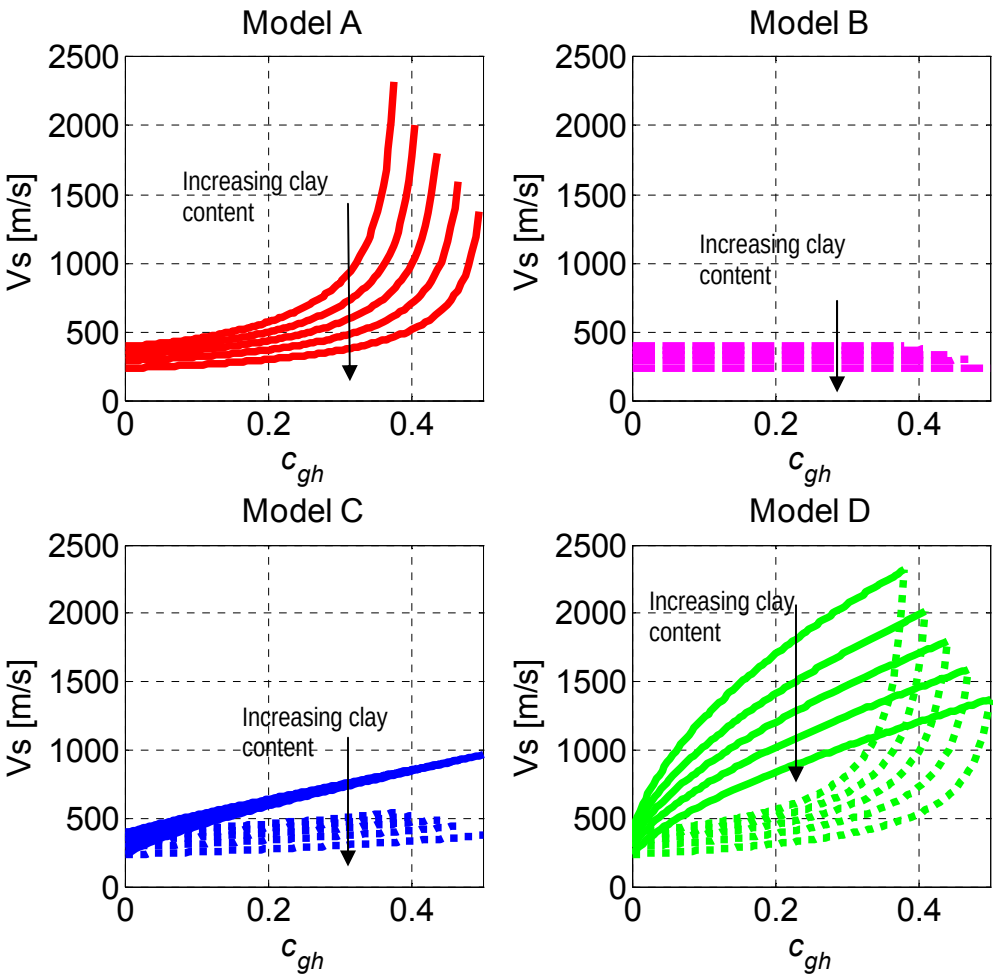

Figure 6: S-wave velocity as a function of the volumetric fraction of hydrate (c_{gh}) in a sediment mixture with variable clay content. **Model A**: load-bearing hydrates disseminated in the sediments; **Model B**: pore-filling hydrates disseminated in the sediments; **Model C**: horizontal or vertical layers of pure hydrates producing slow S-waves (dotted lines) and fast S-waves (solid lines); **Model D**: layers of disseminated, load-bearing hydrates producing slow S-waves (dotted lines) and fast S-waves (solid lines). Different curves correspond to different clay content (from 0 to 100 percent with a 25-percent increment), different critical porosity values, and different coordination numbers. The curves are computed at increasing porosity values as clay content increases. The arrows indicate increasing clay content.

Figure 7 presents the V_P/V_S ratio for the four rock physics models when the clay content is varied. This velocity ratio decreases with hydrate concentration for all models except Model B, which assumes hydrates float in the pores and do not support the shear load. As expected, the V_P/V_S ratio increases with increasing clay content.

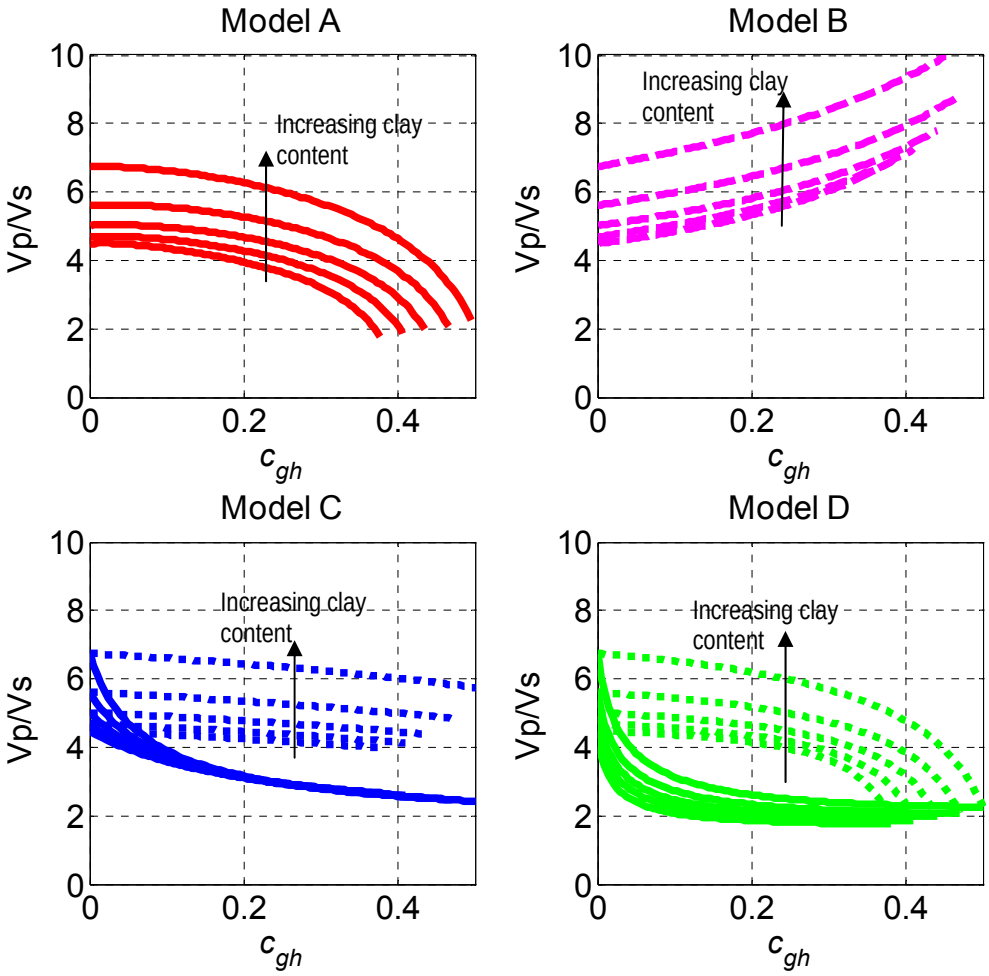

Figure 7: V_P/V_S velocity ratio as a function of the volumetric fraction of hydrate (c_{gh}) in sediment mixtures with variable clay content. **Model A**: load-bearing hydrates disseminated in the sediments; **Model B**: pore-filling hydrates disseminated in the sediments; **Model C**: horizontal or vertical layers of pure hydrates producing slow waves (dotted lines) and fast waves (solid lines); **Model D**: layers of disseminated, load-bearing hydrates producing slow waves (dotted lines) and fast waves (solid lines). Different curves correspond to different clay content (from 0 to 100 percent with a 25-percent increment), different critical porosity values, and different coordination numbers. The curves are computed at increasing porosity values as the clay content increases. The arrows indicate increasing clay content.

The different behaviors of the V_P/V_S ratio for the different rock physics models (Figures 4 and 7) suggest that **amplitude vs. incidence angle** (**AVA**) analyses of P-

waves and converted-S waves may provide valuable insights into hydrate morphologies and concentrations.

P-P and P-SV AVA Modeling: Base of Hydrate Stability Zone

To evaluate the potential value of AVA technology for studying hydrate systems, we simulate the AVA response for P-P and P-SV reflections at an interface between the base of the hydrate stability zone and sediments immediately below that interface that contain free gas (Figure 8). The hydrate systems considered in this AVA modeling are represented by isotropic rock physics Model A and Model B only (Figure 1), which have hydrates disseminated in the host sediments. In Model A, the hydrates are part of the load-bearing frame of the sediments, while in Model B the hydrates fill the pores and do not change the elastic properties of the dry mineral frame. The sediments below the hydrate stability zone are assumed to contain free gas. The elastic properties of this layer are estimated from the rock physics model for unconsolidated sediments presented as Equations 1 through 10.

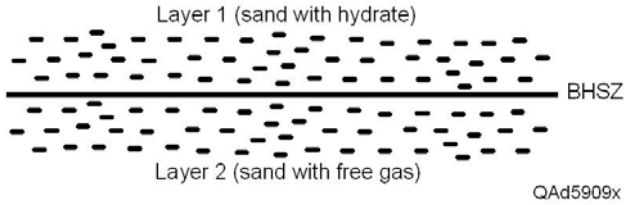

Figure 8: Earth model assumed for base of hydrate stability zone (BHSZ). Porosity is set at 0.37 for both layers.

First we consider the pores of Layer 2 to be 80-percent saturated with free gas, and the remaining pore space to be occupied by brine. We use Reuss (1929) averaging to derive the bulk modulus of the mixture of gas and liquid. We then use Zoeppritz's (1919) equations to derive P-P and P-SV reflectivity as a function of incidence angle.

Figure 9 presents the results for AVA modeling of P-P (left panel) and P-SV (right panel) reflectivity as a function of incidence angle for the model with load-bearing hydrates (Model A). Each curve corresponds to a different hydrate concentration in the upper layer. The arrow indicates increasing hydrate concentration in the pores, which ranges from 0 to 99 percent.

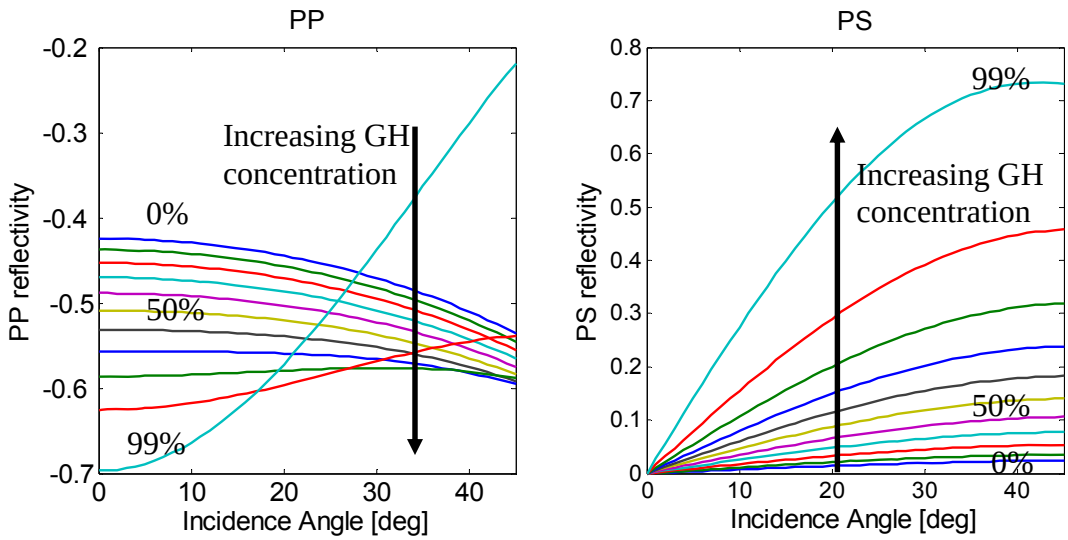

Figure 9: Results of AVA **Model A** showing P-P (left panel) and P-SV (right panel) reflectivity as a function of incidence angle at the interface between the base of the hydrate stability zone and sediments below that contain 80-percent free gas. Each curve corresponds to a different hydrate concentration in the hydrate stability zone. In this model, hydrates are disseminated in Layer 1 (Fig. 8) and are part of the load-bearing frame of the host sediments.

The magnitude of the normal-incidence P-P reflectivity increases with increasing hydrate concentration because the difference between the elastic properties of the hydrate system and the free-gas sediments (lower layer) increases with hydrate concentration. For this model we observe that P-P reflectivity at small incidence angles (near offsets) can better differentiate hydrate concentrations than can P-P reflectivity at larger angles of incidence (far offsets). At small incidence angles, P-P reflectivity becomes brighter as hydrate concentration increases. For small angles, the increase in P-P reflectivity as hydrate concentration increases from 0 to 99-percent is a little more than 60 percent, which should be measurable with good quality seismic data. However, P-P amplitudes increase by only 12 percent when hydrate concentration changes from 0 to 40 percent, which would be difficult to detect with seismic data.

In contrast to P-P reflectivity, if multicomponent seismic data are acquired so that P-SV reflectivity can be measured at incident angles of about 30°, P-SV amplitudes increase by a factor of about 3 as hydrate concentration increases from 0 to 40 percent, and by a factor of more than 30 if hydrate concentration changes from 0 to 99 percent. These amplitude variations should be measurable with reasonable quality multicomponent seismic data.

For hydrate concentrations between 0 and 0.7, the P-P reflectivity curves in Figure 9 are the type associated with Class 3 reservoirs in the Gulf of Mexico, reservoirs for which the reflectivity at zero offset is negative and the AVA gradient is also negative (Roden et al., 2005; Ruger, 2002; Rutherford and Williams, 1989). As hydrate concentration increases beyond 0.7, the P-P AVA behavior shifts to a Class 4 reservoir response, reservoirs for which the reflectivity at zero offset is again negative, but for which there is a positive AVA gradient. The hydrate concentration range that produces these Class 4 reservoir responses corresponds to the hydrate concentration range in

Figure 3 where there is a significant increase in V_S in the layer above the free-gas reservoir. This type of V_S behavior is required for a Class 4 PP AVA response (Castagna and Backus, 1993).

Figure 10 shows the results for AVA modeling of P-P (left panel) and P-SV (right panel) reflectivity as a function of incidence angle in the hypothesis of pore-filling hydrates (Model B). Again, each curve corresponds to a different hydrate concentration in the upper layer of the Earth model (Fig. 8). The arrow indicates the direction of increasing hydrate concentration in the pores, from 0 to 99 percent.

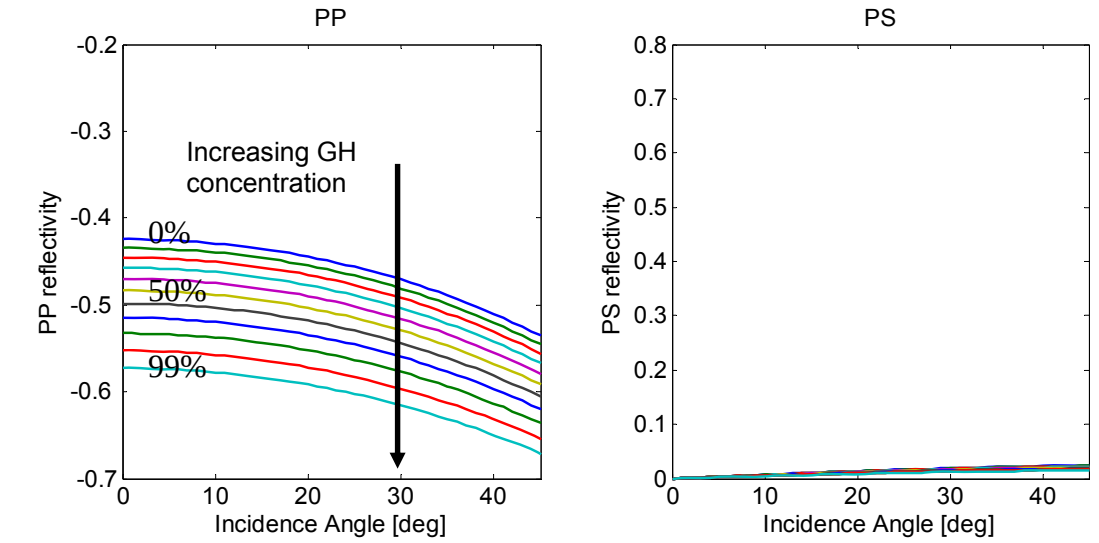

Figure 10: Results of AVA **Model B**. P-P (left panel) and P-SV (right panel) reflectivity as a function of incidence angle at the interface between the base of the hydrate stability zone and sediments below that have a gas saturation of 80 percent. Each curve corresponds to a different hydrate concentration in the upper layer. In this model, hydrates fill the porous space without changing the dry mineral frame of the host sediments.

In the hypothesis of pore-filling hydrates, only P-P reflectivity exhibits any sensitivity to hydrate concentration. All P-P AVA reflectivity curves in Figure 10 are Class 3 responses. It will be challenging to use P-P reflection attributes to identify hydrate concentrations because P-P reflection amplitude increases by only 7 percent when hydrate concentration increases from 0 to 40 percent, and by only a little more than 30 percent if concentration varies from 0 to 99 percent. For this rock physics model, the shear strengths of the sediments containing hydrates do not change with hydrate concentration. Moreover, S-wave velocities in sediments containing pore-filling hydrates and in sediments containing free gas are similar. The only change in V_S is caused by a small density effect. Therefore, in this case, all P-SV reflections are weak and vary little as hydrate concentration increases.

The modeling results presented in Figures 9 and 10 show that P-P reflectivity cannot differentiate between the two hypotheses of hydrate occurrence (load-bearing and pore-filling). The P-P reflectivity curves in Figure 9 (load-bearing assumption) have the same

magnitude and offset dependence as do the curves in Figure 10 (pore-filling assumption). However, P-SV reflectivity for load-bearing hydrates (Model A, Fig. 9) is much different than it is for pore-filling hydrates (Model B, Fig. 10).

In Figures 11 and 12, the free-gas saturation below the **base hydrate stability zone** (**BHSZ**) is 10 percent, rather than 80 percent. The presence of residual gas of 10 percent may be a more plausible scenario than is a well-developed gas reservoir immediately below the BHSZ. As expected, the AVA responses for 10-percent free gas below the BHSZ (Figs. 11 and 12) are similar to the AVA responses for 80-percent free gas (Figs. 9 and 10). The explanation is that small amounts of free gas have the same effect on the seismic velocities as do economical gas saturations. Therefore, it will be challenging to use seismic reflectivity to estimate free-gas saturation below the gas hydrate stability zone.

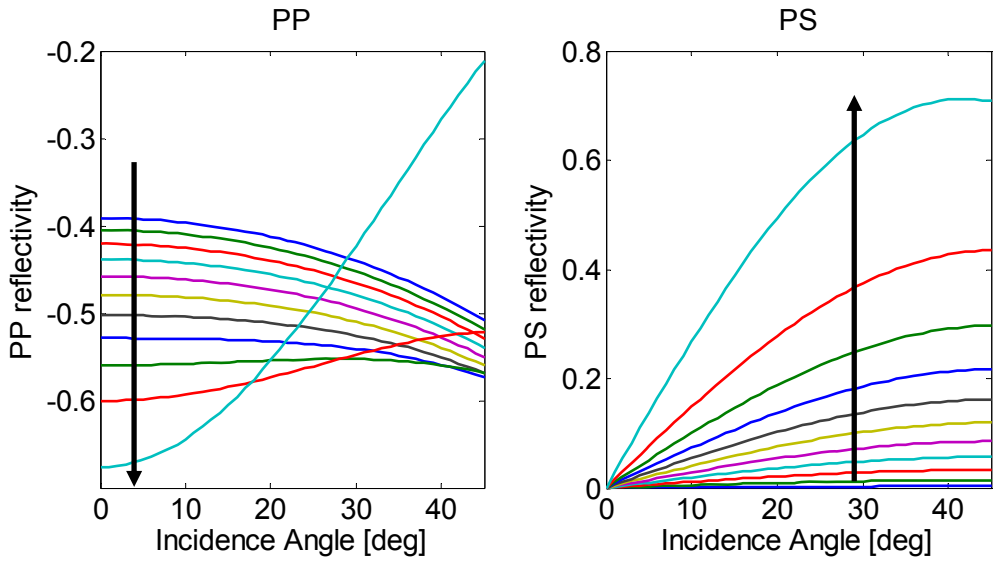

Figure 11: Results of AVA **Model A** showing P-P (left panel) and P-SV (right panel) reflectivity as a function of incidence angle at the interface between the base of hydrate stability zone and sediments below that have a free-gas saturation of 10 percent. Each curve corresponds to a different hydrate concentration in the upper layer. In this model, hydrates are disseminated and are part of the load-bearing frame of the host sediments.

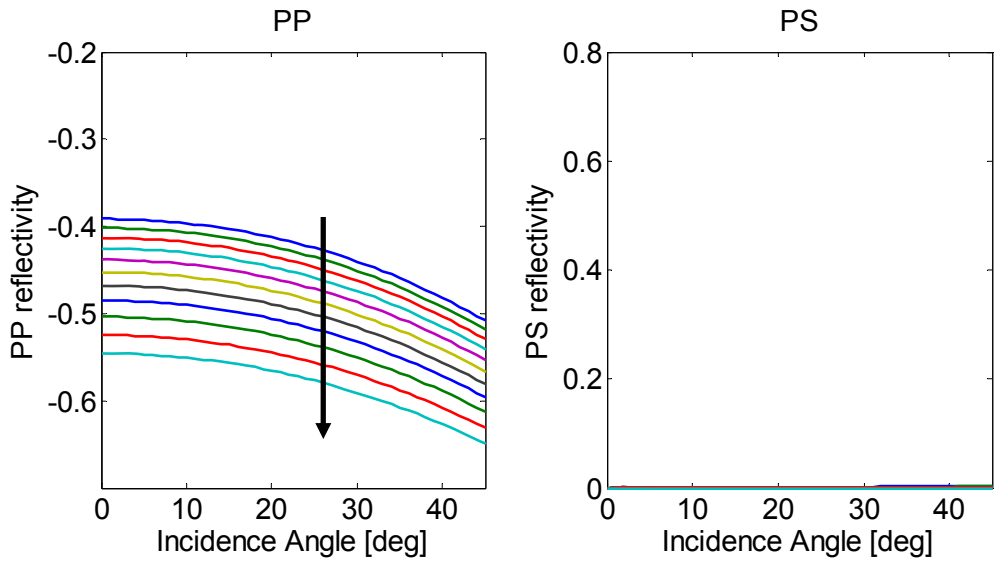

Figure 12: Results of AVA **Model B**. P-P (left panel) and P-SV (right panel) reflectivity as a function of incidence angle at the interface between the base of gas-hydrate stability zone and sediments below that have a free-gas saturation of 10 percent. Each curve corresponds to a different hydrate concentration in the upper layer. In this model, hydrates fill the porous space without changing the dry mineral frame of the host sediments.

This modeling shows that multicomponent seismic technology, and the use of P-SV AVA behavior in particular, can be a powerful tool to understand how hydrates are distributed in relation to their host sediments (load-bearing vs. pore-filling). Using combinations of V_P/V_S ratios and AVA analyses of P-waves and converted PS-waves should improve estimates of deep-water hydrate concentrations.

Next we analyze the behavior of seismic reflection amplitude as a function of incidence angle and azimuth at a hypothetical base of a GHSZ where hydrate is deposited in vertical and aligned fractures/veins (Model C with vertical layers). This hydrate model will generate a transversely isotropic medium with a horizontal axis of symmetry (HTI medium), represented schematically in Figure 13.

We consider the sediments above and below the base of the GHSZ to be clay minerals. In our first example we assume a free-gas residual saturation of 5 percent (Figures 14 and 15). In the second example, we assume no free gas is present below the GHSZ (Figure 16). The porosity of the sediments is 40%. The initial, critical porosity is assumed to be 70 percent, a value observed in local geotechnical data for sediments immediately below the seafloor. The coordination number is 6, and the effective pressure is assumed to be 1MPa.

To model the variation in seismic amplitude from this interface, we use Ruger's (2002) equations for PP and PS reflectivity in two different reflection planes: the isotropy plane and the symmetry-axis plane. The isotropy plane is the plane parallel to the thin vertical hydrate layers; the symmetry-axis plane is orthogonal to the hydrate layers.

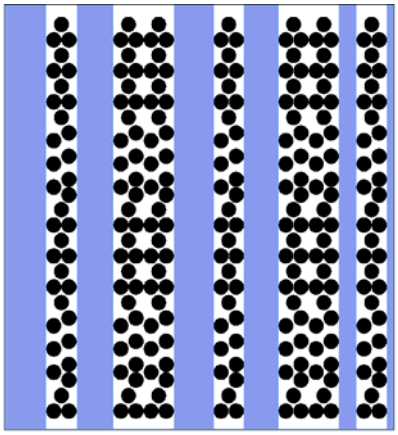

Figure 13: Model C with vertical layers of pure hydrate, which creates a transversely isotropic medium with a horizontal axis of symmetry (HTI medium). This type of medium is azimuthally anisotropic. This model approximates the presence of vertical and aligned fractures/veins filled with pure hydrate.

Figure 14 presents the PP and PS reflectivity modes. The different curves correspond to different hydrate concentration in the sediments, which increases from 0 to 30 percent. The arrows indicate the direction of increasing hydrate concentration. The red curves represent the reflectivity responses as a function of incidence angle in the isotropy plane (parallel to the hydrate vertical layers), and the blue curves represent the reflectivity curves as a function of incidence angle in the symmetry axis plane (orthogonal to the vertical hydrate layers).

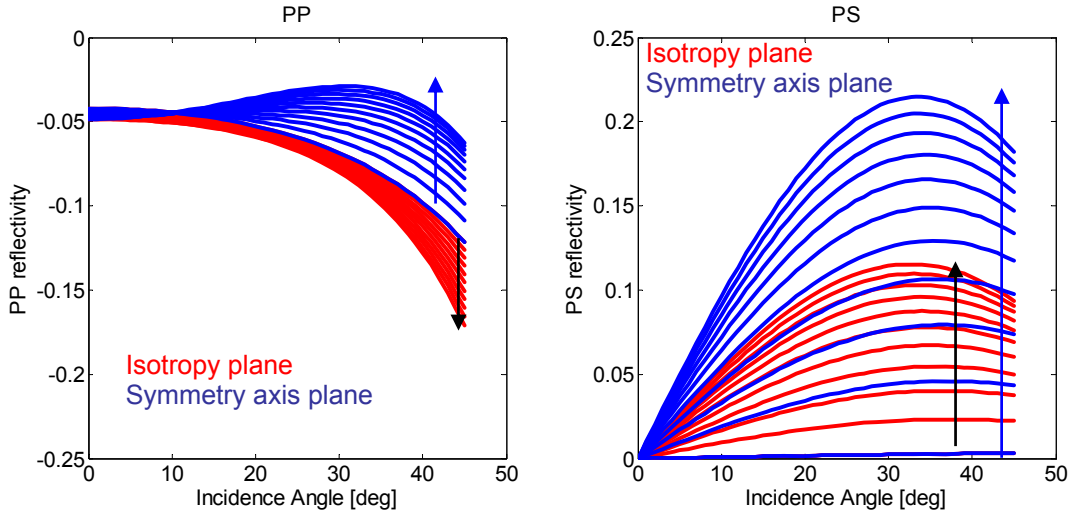

Figure 14: PP (left) and PS (right) reflectivity from the base of the GHSZ for Model C with vertical layers of pure hydrate in the isotropy plane (red curves) and the symmetry-axis plane (blue curves). The different curves correspond to different hydrate concentration in sediments, which increase from 0 to 30 percent. The arrows indicate the direction of increasing hydrate concentration. We assume 5-percent free gas below the GHSZ.

From Figure 14 we can see that PP and PS reflectivites depend on azimuth. The reflectivities in the isotropy plane are different from the ones in the symmetry axis plane.

Also, we observe that as hydrate concentration increases, the PS response becomes stronger than the PP response. This behavior is appealing because the PS mode provides better resolution of near-seafloor geology than does the PP mode.

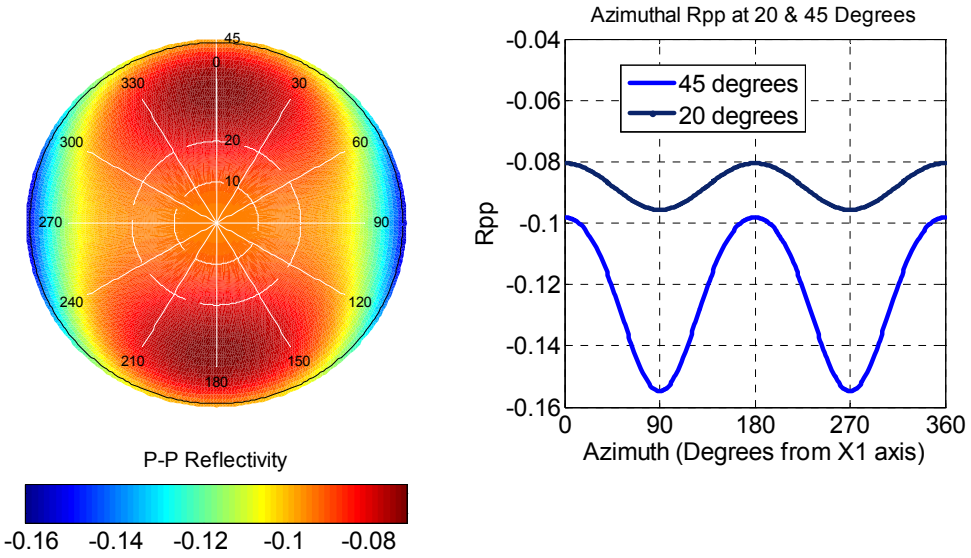

Figure 15: (Left) PP reflectivity as a function of incidence angle (from 0 to 45 degrees) and azimuth (from 0 to 360 degrees). (Right) R_{PP} amplitude variation with azimuth for incidence angles of 20 and 45 degrees. Azimuth 0 is perpendicular to the fracture plane. Vertical hydrate thin layers are oriented E-W.

Figure 15 presents the full azimuthal variation of PP reflectivity from the base of the GHSZ when the hydrate concentration is 20 percent. On the left panel we display PP as a function of all incidence angles (from 0 to 45 degrees) and for all azimuths (from 0 to 360 degrees). On the right panel we represent PP reflectivity as a function of azimuth for incidence angles of 20 and 45 degrees. As we can see in both Figures 14 and 15, the azimuthal variation in PP (and PS) increases with incidence angle.

Figure 16 is similar to Figure 14 except there is no free gas below the GHSZ. By comparing the right-hand panels in Figures 14 and 16 we observe that the PS response does not change whether or not free gas is below the GHSZ. Therefore, we can use the PS mode to quantify hydrate concentration when free gas is present or absent below the GHSZ.

On the other hand, P-wave data are sensitive to fluid changes. Therefore, the PP reflectivity response presented in Figure 16, for which there is no free gas below the GHSZ, differs from the behavior presented in Figure 14 for which there is some residual gas below the GHSZ. The important fact to observe in Figure 16 is that the PP reflections in the isotropy plane (red curves) and the PP reflections in the symmetry axis plane (blue curves) are more or less symmetric about the reflectivity axis. This behavior suggests that if we stack PP data over all azimuths, we will get weak (perhaps no) reflections from the base of the GHSZ. However, on specific 2D lines with azimuths close to the azimuth of the isotropy plane, we may be able to observe a relatively strong PP AVO effect (red curves in Figure 16, left panel).

Our modeling suggests that PS reflections from the base of the GHSZ, especially in the symmetry axis plane are strong, independent of the presence of free gas, and will be the preferred seismic mode for estimating hydrate concentration. We conclude that multiazimuth and multicomponent seismic data are essential for understanding hydrate distribution and concentration.

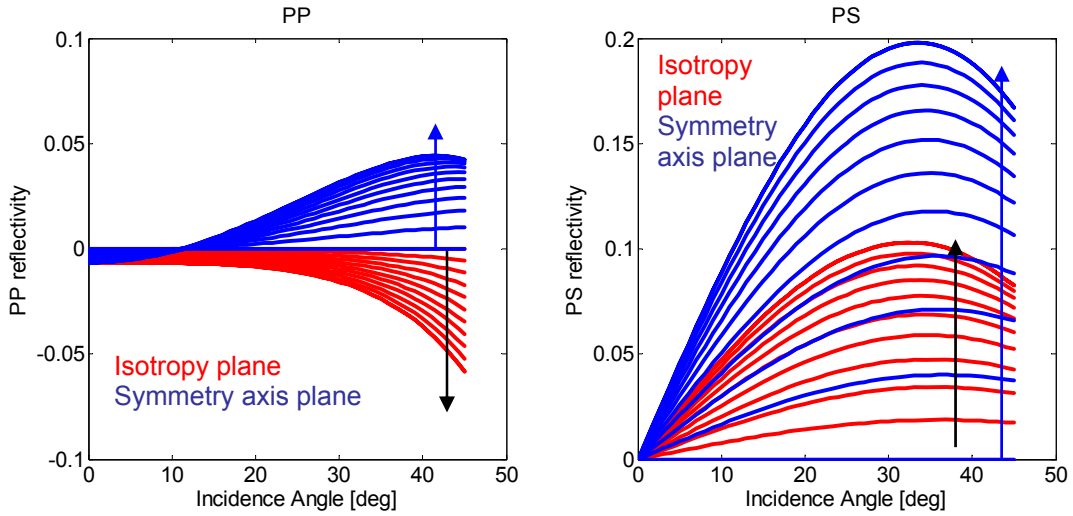

Figure 16: PP (left) and PS (right) reflectivity from the base of the GHSZ for Model C with vertical layers of pure hydrate in the isotropy plane (red curves) and in the symmetry-axis plane (blue curves). The different curves correspond to different hydrate concentration (0 to 30 percent) in the sediments. The arrows indicate the direction of increasing hydrate concentration. We assume NO free gas is present below the GHSZ.

Comparing Rock Physics Modeling Results with Laboratory Measurements

We have compared our rock physics modeling results for Model A with laboratory measurements on synthetic gas hydrates formed in unconsolidated fine sands. Yun et al. (2005) performed laboratory measurements on sediments containing synthetic gas hydrates in concentrations ranging from 0 to 100-percent of the porous space. For hydrate concentration smaller than 100 percent, the remaining pore space was occupied by brine. The porosity of the sand samples was 0.37. The laboratory measurements were performed at low effective pressure, smaller than 0.01 MPa.

In Figures 13 and 14 we compare their laboratory measurements for P- and S-wave velocity as a function of hydrate concentration in the pores with our results for rock physics Model A (load-bearing hydrates). The left panels in these figures show the lab measurements and the right panels show our rock physics modeling results. The unconsolidated sediments in the rock physics model are represented by quartz grains at critical porosity, assumed to be 0.37, the same value as the porosity of the sand samples used in the laboratory measurements.

Figure 13 shows that P-wave velocity increases with hydrate concentration for both lab measurements and for our rock physics model of load-bearing hydrates. The increase in P-wave velocity is non-linear and is larger when hydrate concentrations in the pores exceed 50 percent. For hydrate concentrations smaller than 50 percent, the increase in P-wave velocity due to the presence of hydrates is small. We observe a good agreement between the laboratory measurements of P-wave velocity as a function of hydrate concentration and our rock physics modeling results.

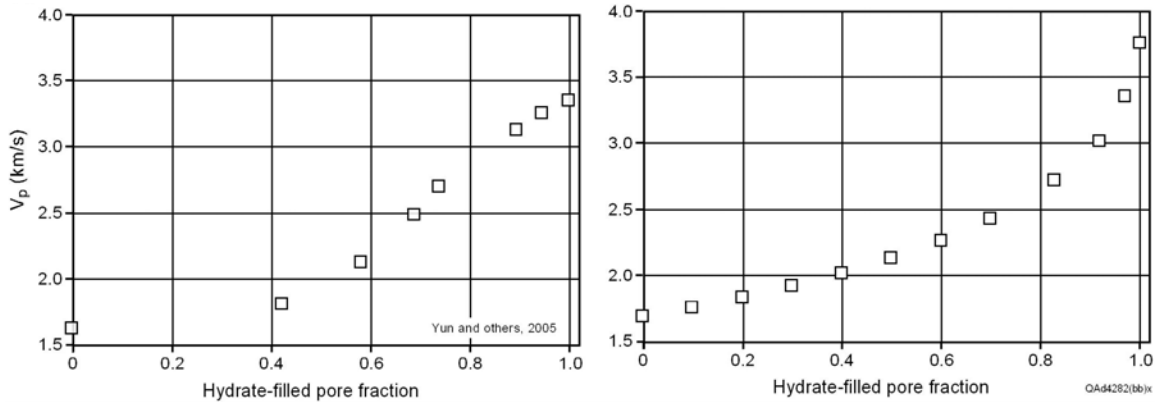

Figure 13: Comparison of laboratory and **Model A** results for P-wave velocities as a function of hydrate concentration in the pores. *Left panel*: Yun et al. (2005) lab results. *Right panel*: Our rock physics modeling results when hydrates are assumed to be part of the dry frame of the sediments.

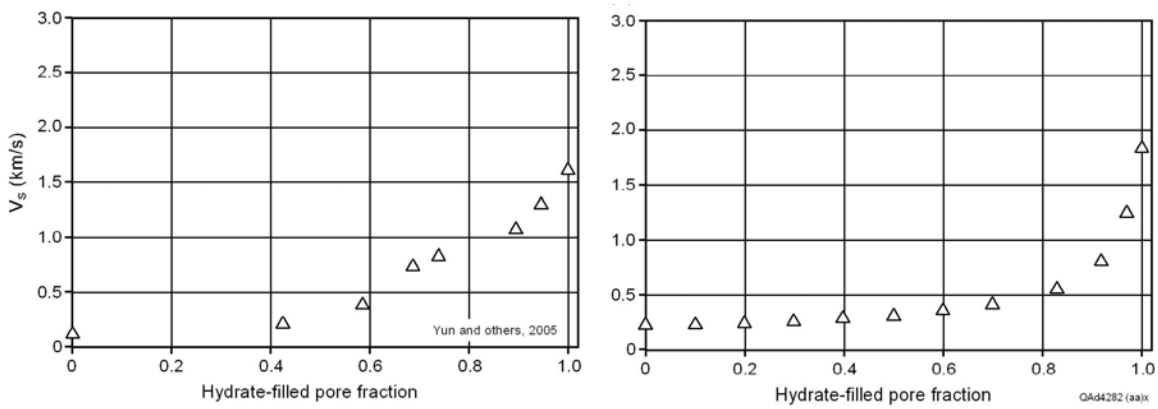

Figure 14: Comparison of laboratory and **Model A** results for S-wave velocities as a function of hydrate concentration in the pores. *Left panel*: Yun et al. (2005) lab results. *Right panel*: Our rock physics modeling results when hydrates are assumed to be part of the dry frame of the sediments.

Figure 14 shows how S-wave velocity increases with hydrate concentration for the Yun el al. (2005) lab measurements and for our rock physics model of load-bearing hydrates. The increase in S-wave velocity is large when the hydrate concentration in the pores exceeds 50 percent. For hydrate concentrations smaller than 50 percent, the increase in S-wave velocity due to the presence of hydrates is small. We observe a relatively good agreement between the laboratory measurements of S-wave velocity as a function of hydrate concentration and our rock physics modeling results.

Based on the agreement between these lab data and our rock physics modeling results, we conclude our rock physics theory is sound and will be a valuable diagnostic tool as we proceed to determine interval seismic-based values of V_P and V_S near the seafloor across our study areas.

As an additional comment on the validity of using our Model A to interpret hydrate concentrations in hydrate-sediment mixtures, Winters et al. (2004) studied samples containing natural gas hydrates from the Mallik 2L-38 well, Mackenzie Delta, and found that these naturally formed gas hydrates were part of the load-bearing frame of their host sediments.

However, Winters et al. (2004) also performed measurements on Ottawa sands containing synthetic methane hydrate formed in the laboratory. These measurements suggest that hydrates cement their host sediments. A cementation hypothesis implies a large increase in P- and S-wave velocities for small hydrate concentrations (Dvorkin et al., 1994; Ecker et al., 1998). This type of velocity behavior is not usually observed in published field data acquired across hydrate zones. This Winters et al. (2004) laboratory study presents an apparent contradiction between the hydrate-sediment morphology associated with naturally-forming hydrates, which appear to be part of the load-bearing frame and do not cement the grains, and laboratory-formed hydrates, which appear to cement the grains of the host sediments.

Based on our rock physics results using Model A, we observe that the Yun et al. (2005) laboratory measurements on synthetic gas hydrates (Figures 13 and 14, left panels) are in qualitative agreement with Winters et al. (2004) laboratory observations on naturally formed gas hydrates. Both studies suggest that a load-bearing hypothesis is appropriate for hydrates that are uniformly distributed throughout their host sediments.

More laboratory and field measurements are needed to understand the complex mechanisms of hydrate formation and distribution in sediments. Probably different hydrate/sediment morphologies apply in different natural settings.

Conclusions

We have developed rock physics models for unconsolidated sediments that host hydrates in deep-water, near-seafloor strata and that are characterized by large V_P/V_S ratios. We have described four possible rock physics models for such hydrate systems in which we assume various morphologies for the hydrates and their host sediments. Modeling results show that the elastic properties of hydrate-bearing units depend on the geometrical details of the hydrate distribution within the sediments. We have not developed a rock physics model for hydrates that fill thin vertical fractures and dikes,

which is a fifth possible hydrate-sediment morphology. We will eventually expand our rock physics modeling to encompass vertical-void-filling hydrates.

We find good agreement between our theoretical predictions for P- and S-wave velocities in a medium of load-bearing hydrate (our Model A) and laboratory measurements on synthetic gas hydrates in unconsolidated sands. There are other laboratory data performed on naturally-formed gas-hydrates from the Mallik well, Mackenzie Delta, (Winters et al, 2004) that also suggest a load-bearing hypothesis is appropriate for hydrate occurrence within sediments. We conclude that, in some natural environments, hydrates are a part of the dry mineral frame of their host sediments. However, more laboratory and field studies are needed to understand the complex mechanisms of hydrate formation in sediments. These mechanisms may require that different hydrate/sediment morphologies be used from site to site, depending on specific in-situ conditions.

In some deep-water environments there may be layered types of sediment/hydrate morphologies. Our modeling shows that in such media, the effective elastic properties of stratified near-seafloor sediments containing hydrates may be anisotropic, and in such cases, the acquisition of fast and slow components of multicomponent seismic data has great value. If the layering is vertical, approximating steeply dipping and aligned fractures filled with hydrates, the effective elastic properties will be azimuthally anisotropic.

AVA modeling indicates multicomponent seismic technology can be important for understanding how hydrates are distributed in relation to their host sediments and for estimating hydrate concentrations. Using combinations of P-P and P-SV AVA reflectivity, P- and S-wave interval velocities, and V_P/V_S ratios should improve our understanding of deep-water hydrate systems. When hydrates form in steeply dipping and aligned fractures, our modeling suggests that multiazimuth and multicomponent 3-D seismic data are essential for understanding and quantifying hydrate distributions.

References

Backus, G., 1962, Long-wave elastic anisotropy produced by horizontal layering, J. Geophys, Res., 76, 4427-4440.

Backus, M.M., Murray, P.E., Hardage, B.A., and Graebner J., 2006, High-resolution multicomponent seismic imaging of deepwater gas-hydrate systems, The Leading Edge, V. 25, No5, 578-596.

Carcione, J. M. and Tinivella, U., 2000, Bottom-simulating reflectors: Seismic velocities and AVO effects, Geophysics, 65, No.1, 54-67.

Castagna, J. P. and Backus, M. M., 1993, Offset-dependent reflectivity: Theory and practice of AVO analysis, Society of Exploration Geophysicists, 348p.

Chand, S., Minshull, T.A., Gei, D., and Carcione, J.M., 2004, Elastic velocity models for gas-hydrate-bearing sediments-a comparison, Geophys. J. Int., 159, 573-590.

Collet, T.S., 1998, Well log evaluation of gas hydrate saturations, Transactions of the Society of Professional Well Log Analysts 39th Annual Logging Symposium, Paper MM.

Digby, P. J., 1981, The effective elastic moduli of porous granular rocks. J. Appl. Mech., 48, 803-808.

Dvorkin, J., Nur, A., and Yin, H., 1994, Effective properties of cemented granular material: Mechanics of Materials, 18, 351-366.
Dvorkin, J., and Nur, A. 1996, Elasticity of high-porosity sandstones: theory for two North Sea data sets, Geophysics, V.61, 1363-1370.
Dvorkin, J., Prasad, M., Sakai, A., and Lavoie, D., 1999, Elasticity of marine sediments, Geophys. Research Lett., 26, 1781-1784.
Ecker, C., Dvorkin, J., Nur, A., 1998, Sediments with gas hydrates: Internal structure from seismic AVO, Geophysics, V.63, No.5, 1659-1669.
Ecker, C., Dvorkin, J., and Nur., A., 2000, Estimating the amount of gas hydrate and free gas from marine seismic data, Geophysics, 62, No. 2, 565-573.
Gassmann, F., 1951, On the elasticity of porous media, Vier. Der Natur. Gesllschft in Zurich, 96, 1-23.
Hardage, B.A., Roberts, H.H., Murray, P.E., Remington, R., Sava, D.C., Shedd W., Hunt, J. Jr., 2007, Multicomponent seismic technology assessment of fluid-gas expulsion geology: Gulf of Mexico, *in* Collett, T., Johnson, A., Knapp, C., and Bosswell, R., eds., Natural Gas Hydrates: Energy Resource Potential and Associated Geologic Hazards: AAPG Special Publication.
Hashin, Z., and Shtrikman, S., 1963, A variational approach to the elastic behavior of multiphase materials, J. Mech. Phys. Solids, 11, 127-140.
Helgerud, M.B., Dvorkin, J., and Nur, A., Sakai, A., and Collet, T., 1999, Elastic-wave velocity in marine sediments with gas hydrates: Effective medium modeling, Geophys. Res. Lett., 26, 2021, 2024.
Hill, R. 1963, Elastic properties of reinforced solids: some theoretical principles, J. Mech. Phys. Solids, 11, 357-372.
Holbrook, W.S., H. Hoskins, W.T. Wood, R.A. Stephen, D. Lizarralde, & Leg 164 Scientific Party, 1996. Methane hydrate and free gas on the Blake Ridge from vertical seismic profiling. Science 273, 1840-1843.
Kleinberg, R.L. and Dai, J., 2005, Estimation of the mechanical properties of natural gas hydrate deposits from petrophysical measurement, OTC 17205, Offshore Technology Conference, Houston, TX, 2-5 May 2005.
Lee, M.W., Hutchinson, D.R., Collet, T.S., and Dillon, W.P., 1996, Seismic velocities for hydrate bearing sediments using weighted equation, J. Geophys. Res., 101, 20, 347-358.
Lu, S. and McMechan, G.A., 2002, Estimation of gas hydrate and free gas saturation, concentration, and distribution from seismic data, Geophysics, 67, no.2, 582-593.
Lu, S. and McMechan, G.A., 2004, Elastic impedance inversion of multichannel seismic data from unconsolidated sediments containing gas hydrate and free gas, Geophysics, Vol. 69, No1, 164-179.
Mavko G., Mukerji, T., Dvorkin, J., 1998, The rock physics handbook, Cambridge University Press.
Miller, J. J., Lee, M.W., von Huene, R., 1991, An analysis of seismic reflection from the base of a gas hydrate zone, offshore Peru, AAPG Bulletin, 75, 910-924.
Mindlin, R.D., 1949, Compliance of elastic bodies in contact, J. Appl. Mech., 16, 259-268.
Murphy, W.F., 1982, Effects of microstructure and pore fluids on the acoustic properties of granular sedimentary materials, Ph. D. dissertation, Stanford University.

Murray, D.R., Kleinberg, R.L., Sinha, B.K., Fukuhara, M., Osawa, O., Endo, T. and Namikawa, T., 2006, Saturation, acoustic properties, growth habit, and state of stress of a gas hydrate reservoir from well logs, Petrophysics, Vol. 47, No.2, 129-137.

Pearson, C.F., Hallek, P.M., McGuire, P.L., Hermes, R., and Mathews, M., 1983, Natural gas hydrate deposits: a review of in-situ properties, Journal of Physical Chemistry, 87, 4180-4185.

Prasad, M., and Dvorkin, J., 2001, Velocity to porosity transform in marine sediments, Petrophysics, 42, 5, 429-437. 89.

Reuss, A., 1929, Berechunung der fliessgrense von mischkristallen auf grund der plastizitatsbedinggung fur einkristalle, Zeitschrift fur Angewandte Mathematik and Mechanik, 9, 49-58.

Roden, R., Forrest, M., and Holeywell, R., 2005, The impact of seismic amplitudes on prospect risk analysis, The Leading Edge, 24, 706-711.

Ruger, A., 2002, Reflection coefficients and azimuthal AVO analysis in anisotropic media, Geophysical Monograph Series No. 10, Society of Exploration Geophysicists, Tulsa, OK, 189 pages.

Rutherford, S.R., and Williams, R.H., 1989, Amplitude-versus-offset in gas sands, Geophysics, 54, 680-688.

Sloan, E.D., 1998, Clathrate hydrate of natural gas, 2nd ed.: Marcel Dekker.

Walton, K., 1987, The effective elastic moduli of a random packing of spheres, J. Mech. Phys. Solids, 35, 213-226.

Waite, W.F., Winters, W.J., Mason, D.H., 2004, Methane hydrate formation in partially water-saturated Ottawa sand, American Mineralogist, 89, 1202-1207.

Winters, W. J., Pecher, I.A., Waite, W.F., Mason, D.H., 2004, Physical properties and rock-physics models of sediment containing natural and laboratory-formed methane gas hydrate, American Mineralogist, 89, 1221-1227.

Wood, W.T., Stoffa, P.L., and Shipley, T.H., 1994, Quantitative detection of methane hydrate through high-resolution seismic velocity analysis, Journal of Geophysics Research, 99, 9681-9695.

Yuan, T.S., Hyndman, G.D., Spence, G.D., and Desmons, B., 1996, Seismic velocity increase and deep-sea gas hydrate concentration above a bottom-simulating reflector on the northern Cascadia continental slope: J. Geophys. Res., 101, 13655-13671.

Yun, T.S., Francisca, F.M., Santamarina, J.C., Ruppel, C., 2005, Compressional and shear wave velocities in uncemented sediment containing gas hydrate, Geophysical Research Lett., 32, L10609-L10613.

Zimmer, M.A., 2003 Controls on the seismic velocities of unconsolidated sands: Measurements of pressure, porosity and compaction effects, Ph. D. Thesis, Stanford University.

Zoeppritz, K., 1919, Erdbebenwellen VIIIB, On the reflection and propagation of seismic waves. Gottinger Nachrichten, I, 66-84.

Acronyms and Abbreviations

AVA: Amplitude versus angle
$\mathbf{c_{gh}}$: hydrate concentration
BHSZ: base hydrate stability zone
f: volume fraction
G: shear modulus
K: bulk modulus
$\mathbf{V_P}$: P-wave velocity
$\mathbf{V_S}$: S-wave velocity
Φ: porosity
ρ: density